Modeling and design of millimeter wave gyroklystrons*

B. Levush,[†] M. Blank, J. Calame, B. Danly, K. Nguyen,[a)] D. Pershing,[b)] S. Cooke,[c)]
P. Latham,[d)] J. Petillo,[c)] and T. Antonsen, Jr.[e)]
Naval Research Laboratory, Washington, DC 20375

A series of high power, high efficiency K_a-band and W-band gyroklystron experiments has been conducted recently at the Naval Research Laboratory (NRL). Stagger tuning of the cavities for bandwidth enhancement is commonly used in the conventional multicavity klystrons. The desired stagger tuning is usually achieved via mechanical tuning of the individual cavities. However, in the millimeter wave regime, particularly, in the case of the high average power operation, it is desirable to be able to achieve the required stagger tuning by design. The NRL gyroklystron experiments explored the tradeoffs between power, bandwidth, efficiency, and gain to study the effects of large stagger tuning in millimeter wave without resorting to mechanical tuning of the cavities. Both, K_a-band and W-band, experiments demonstrated a record power-bandwidth product. The success of the experiments was due in large part to a battery of improved large-signal, stability, and cold test codes employed in the modeling and design stage. Theoretical models that provide the basis for these design simulation tools and the design methodology will be presented. © *1999 American Institute of Physics.* [S1070-664X(99)92905-1]

I. INTRODUCTION

Gyroklystrons in K_a-band and W-band are attractive sources for the next generation of millimeter wave radars.[1] This is because gyroklystrons are capable of operating at both high peak power and high average power with high efficiency at these frequencies.[2] The instantaneous bandwidth of gyroklystrons is determined by the quality factor (Q) of the cavities, and especially by the Q of the output cavity. This leads to narrow bandwidth, since the Q is typically on the order of 150–300. However, it is possible to increase the bandwidth by employing a multicavity gyroklystron circuit, with each cavity tuned to a different frequency (stagger tuning). Stagger tuning of the cavities for bandwidth enhancement is commonly used in conventional multicavity klystrons. The desired stagger tuning is usually achieved via mechanical tuning of the individual cavities. However, in the millimeter wave regime, particularly, in the case of the high average power operation, it is desirable to be able to achieve the required stagger tuning by design. Therefore, the purpose of our investigations is to develop and validate the simulation models, the design methodology, and the manufacturing procedure to achieve this goal for high power gyroklystrons. In this paper we describe the simulation models and the design procedure to address the relevant issues.

A series of experiments has been conducted recently at

the NRL to study the effects of large stagger tuning on the performance of the gyroamplifiers. These experiments explored the tradeoffs between power, bandwidth, efficiency, and gain due to circuit geometry and operating parameter variation. The K_a-band experiments, using a three-cavity[3] circuit with heavy stagger tuning, demonstrated more than double the bandwidth of the two-cavity circuit,[4] with only a modest decrease in efficiency. The W-band experiments achieved a record power-bandwidth product in a four-cavity gyroklystron circuit with large stagger tuning.[5,6] For all experiments the results are in excellent agreement with simulations.

Extensive theoretical work has produced a hierarchy of nonlinear models to describe the beam-wave interaction in the gyroklystron circuit. The validity of these models and their accuracy will be discussed in Sec. II. Ensuring stable operation is a central step in the gyroklystron design procedure. Issues relevant to self-oscillations in the drift sections of the gyroklystron circuit will be discussed in Sec. III. The design procedure of the input coupler will be described in Sec. IV. Finally, in Sec. V the simulation results are compared with the experimental data and the methodology developed for designing the high average power W-band gyroklystron is briefly discussed.

II. THEORETICAL MODEL

The combination of the phase bunching due to the cyclotron maser instability in a cavity and the ballistic phase bunching in drift tubes makes the gyroklystron capable of operating at high efficiency, high power, and high gain. Several models describing the gyroklystron interaction have been developed over the years, ranging from an analytical "point-gap" approach[7] to a multimode, self-consistent ap-

proach implemented in a simulation code.[8] A complete description of the variety of theoretical models, approaches, and methods is beyond the scope of this paper. In this section we will describe briefly the theoretical models, which have been implemented in the large signal codes used at the Naval Research Laboratory (NRL) for designing the gyroklystron experiments.

We started from the model described by P. Latham *et al.*[9] The assumptions in that model were dictated by the intended gyroklystron application, drivers for the next generation of linear colliders for particle physics research. The collider application required a narrow band, low average power gyroklystron capable of producing a very high peak power with high efficiency. This was achieved by using a moderately relativistic 500 kV and 200 A electron beam.[10] The NRL gyroklystron development is driven by a radar application, which requires operation at high average power and wide bandwidth, while maintaining relatively high peak power and efficiency.[11] This can be achieved by using a weakly relativistic electron beam (50–70 kV and 4–10 A) in a stagger-tuned multicavity circuit.

It turns out that the model in Ref. 9, when augmented with additional capabilities required for the design of multicavity gyroklystron with stagger tuning for bandwidth enhancement, contains essentially all of the effects needed for an adequate description of the beam-wave interaction in a gyroklystron. Specifically, a more accurate model of the input coupler and a model for calculating the dielectric loading of the intermediate cavities have been added. In addition, it turned out that the procedure for designing a gyroklystron amplifier used in Ref. 9 is not suitable for effective evaluation of the bandwidth of the circuit. This deficiency was

removed as well. All of these efforts resulted in a new procedure for designing wide band gyroklystrons and to an improved version of the large signal code, which we named MAGYKL. Here we will describe only the additions to the model, keeping the same notation as Ref. 9.

We start with the evolution of the complex amplitude in each cavity in MAGYKL, which is described by a time-dependent equation

$$\frac{\partial a}{\partial \tau} + \left(\frac{1}{2} + i\Delta_\omega\right)a = -\frac{Q_l}{2\omega W_{EM}}\int dx^3 \int_0^T \frac{dt}{T} J^* E_c^* e^{i\omega t}, \quad (1)$$

where a is the complex normalized amplitude of the fields; $\Delta_\omega = Q_l\{\text{Re}\{\omega_c\} - \omega\}/\omega$ is the normalized frequency shift, Q_l is the load quality factor of the cavity, ω is the drive frequency, and ω_c is the cold resonant frequency, $\mathbf{J}$ is the beam current density, W_{EM} is the field stored energy, $\mathbf{E}_c$ is the cold cavity electric field, J is current density, $T \equiv 2\pi/\omega$ is the period, and τ is the slow time[12] normalized to Q_l/ω. Note that in the original formulation (Ref. 9), Eq. (1) does not contain the time derivative. We will come to this point later when addressing the design procedure.

The cavities are modeled by a series of straight uniform sections with abrupt radial discontinuities at the junctions. The fields in each section, expanded as a radial series of TE, TM, and TEM modes, are determined through a scattering matrix solution.[13] In order to accurately predict the amplifier bandwidth of the amplifier, the input cavity model used in the past was modified to include a frequency-dependent electric field amplitude in the drive cavity, as dictated by the resonant frequency and total Q of the input cavity. The field amplitude in the drive cavity is given by

$$|a|^2 W_{EM} = P_{\text{in}}\frac{\omega}{Q_{\text{ext}}} \frac{1}{\left|\omega - \omega_c + \frac{i\omega}{2}\left(\frac{1}{Q_{\text{ext}}} + \frac{1}{Q_{\text{losses}}}\right) + \frac{1}{a}\frac{I_b}{2W_{EM}}\int d\xi \frac{c}{\omega}\left\langle\frac{\nu_{\text{perp}} \cdot E_c e^{-i\omega t}}{\nu_z}\right\rangle\right|^2}, \quad (2)$$

where P_{in} is the input power, which is assumed to be frequency independent, Q_{external} is the external quality factor, Q_{losses} is the quality factor which includes ohmic and any other losses from the input cavity, such as field leakage through the beam tunnel, $\nu_\perp$ and ν_z are the perpendicular and axial electron velocities, $\xi = z\omega/c$ is the normalized distance, and the angle brackets denote an average over particles. In the derivation of Eq. (2), we assumed that the electric field in the input cavity is small enough that the beam-wave interaction can be evaluated in the linear regime.

Before describing the design procedure, a few remarks concerning usage of "reduced models" are in order. It was originally expected that the model used in Ref. 9 was unnecessarily detailed for a weakly relativistic and low current beam. Therefore a reduced model[14] based on a single mode sinusoidal or Gaussian axial profile for the "cold" field

could be used. Although reduced models of gyroklystron amplifiers are still useful for understanding the basic operation of these devices, they are not adequate as a design tool if the combination of the highest possible bandwidth and efficiency is desired. We illustrate the limitations of the reduced models by comparing the results produced by these models with our improved large signal code, MAGYKL. We will use the four cavity W-band gyroklystron with stagger tuning as an example. If the "cold field" in the cavities is represented only by one radial mode, TE_{01}, and the axial profile is sinusoidal, the output power versus input power (the transfer function) will be significantly different from the transfer function predicted by MAGYKL. This is shown in Fig. 1. Similarly, the power versus frequency dependence (bandwidth curve) at saturation as predicted by MAGYKL is quite different from the prediction of a model based on a single mode sinusoidal or Gaussian axial profile for the "cold" field.
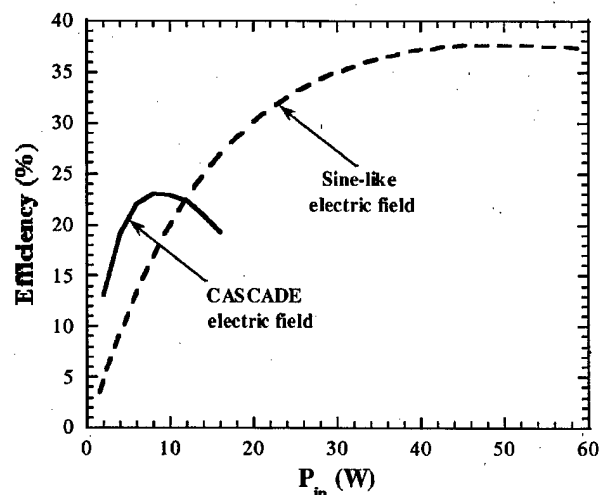
FIG. 1. Efficiency versus input power in the case of four-cavity gyroklystron. The four-cavity structure with the following parameters: Cavity 1 f_c=93.4064 GHz, Q_{ext}=150, Q_{loss}=800; Cavity 2 f_c=94.2063 GHz, Q_{loaded}=175; Cavity 3 f_c=93.2836 GHz, Q_{loaded}=175; Cavity 4 f_c=93.8874 GHz, Q_{loaded}=162.43; electron beam parameters are: V=65 kV, I=6A α=1.5, guiding center radius r_g=0.081 cm, zero velocity spread. Magnetic field was optimized for maximum efficiency, B=36.8 kG.

A. Design procedure

The process of using MAGYKL for designing a gyroklystron is a multistep procedure, which includes the choice of an electrodynamical structure, the electron beam and drive signal parameters, and the optimization of device performance by varying the magnetic field. The determination of the electrodynamical structure consists of several steps. First, the resonance frequency, Q, and length for each cavity are chosen. Based on this information, CASCADE[13] is used to determine approximate cavity shapes and sizes and the drift tube radii that yield the desired frequencies and Q's as well as the electric field profile, $E_c(r,z)$. The field axial profile and the amplitudes and phases of the modes together with the "cold" frequencies and Q's are used in the large signal code MAGYKL, in which the particle equations and the wave amplitude Eq. (1) are solved. At this point the input cavity parameters, such as drive frequency, P_{in}, Q_{ext}, and Q_{loss}, the beam parameters, such as current, voltage, $\alpha = v_\perp / v_z$, root-mean-square (rms) velocity spread and the guiding center radius, and the magnetic field value are chosen.

The amplitude in the input cavity is determined by Eq. (2) via iterations. Usually, three to five iterations are sufficient. The number of the time steps needed for the amplitude, a, for the cavities other than the input to reach a steady-state solution is usually on the order of 100. The overall efficiency is evaluated using this steady-state amplitude. Note that the steady-state solution is consistent with the prescribed total quality factor.

In the original version of the large signal code,[9] without the time derivative term, the values Q and the magnitude and phase of the complex amplitude a and its phase and Q were used to determine Δ_ω from the energy balance equation, as

in Eq. (7) in Ref. 9. This approach proved to be computationally effective for the cases studied in Ref. 9. However, it turned out to be not practical when stagger tuning was employed for both efficiency and the bandwidth optimization. Adding the time derivative did not change the nature of the final solution, since the complex amplitude has to reach a steady state in order to satisfy the power balance equation. However, the numerical implementation of solving Eq. (2) is such that the amplitude and phase of the wave are adjusted from one time step to another automatically until the power balance equation is satisfied. The computation is repeated for different values of the magnetic field in order to optimize the performance. Note that the drift length is mainly determined by the gain or efficiency optimization.

The choice of the guiding center radius involves additional considerations. On the one hand, it is desired to make the field of the operating mode evanescently small in the drift region, hence a small drift tube radius is advantageous. On the other hand, the beam size has to be adequate to ensure maximum coupling to the electric field and minimum interception by the drift walls. Usually a distance on the order of three Larmor radii from the drift wall is considered to be safe. Another interesting point worth mentioning concerns the adequacy of the small Larmor radius approximation that is typically used for describing the beam-wave interaction in the weakly relativistic regime. We find that if the small Larmor radius approximation is used, the frequency pulling due to the beam loading is about 50 MHz different from MAGYKL calculations (no small Larmor radius approximation is used in Bessel function evaluation in the equations used in MAGYKL). By itself it is a tiny error, but considering the fact that the stagger tuning of the cavities is on the order of 100–150 MHz, the 50 MHz error is quite significant.

B. Effects of the dielectric insert

The total quality factors for the intermediate cavities are assumed known in our model. In practice, in order to realize the required cavity losses, a ring of a lossy dielectric is inserted into the cavities. MAGYKL requires prior calculation of the field eigenmode profiles for each cavity, which are normally obtained from the scattering matrix code CASCADE, which does not allow the ceramic insert to be included in the computation. Therefore some approximation was necessary to model the actual device. Using MAGYKL, a design begins with a set of frequency and Q values for each cavity, and a known dielectric constant for the ceramic inserts.

An unpublished code, DIELEC, developed by P. Latham and modified by B. Levush and A. Berman, is used for each cavity to find dimensions (radius, length of the dielectric ring). DIELEC is a more advanced scattering matrix code that permits (lossy) ceramic rings in the description of the cavity geometry. Loss is included through the use of complex values of the dielectric constant. The cavity frequency and Q obtained are passed as inputs to MAGYKL. Note that, when DIELEC is used, the number of modes required to converge on the eigenfrequency is about 10. However, since CASCADE must be used for the field profiles passed to MAGYKL, approximate profiles are computed with the assumption that the

cavity electromagnetic fields are excluded from the dielectric ring as if it were metal. This assumption is valid if the real part of the dielectric constant of the ceramic is large. Cavity dimensions for this equivalent cavity are kept the same as those of the true cavity, except that the radius used in CAS-CADE is adjusted slightly to match the required resonant frequency. We have recently adapted MAGYKL to take fields from DIELEC. Detailed description of the model will be presented in other publications. The adapted code, MAGYKL-C, follows a similar algorithm, but instead of requiring an approximate equivalent cavity to be constructed, the field profile is taken directly from DIELEC. The cavity frequency and Q are therefore fully consistent with the cavity and dielectric dimensions, so that a level of approximation has been removed from the calculation.

The original code MAGYKL has been used successfully in the design of NRL gyroklystron experiments using the cavity field approximation described, and therefore for the parameter regime of those experiments the approximation of field exclusion from the dielectrics seems most likely valid. Here we explore this validity by comparing results based on the original model with the more complete model, and extend the comparison to other parameter regimes of experimental interest. We will consider two cases of dielectric properties: (A) large dielectric constant, high loss ($\varepsilon = 12.24 - i3.67$) and (B) large dielectric constant, moderate loss ($\varepsilon = 10.0 - i0.88$). MAGYKL has been used successfully in the design of devices in the case "A" regime, taking the field profile as if the ceramic were metal. Case "B" requires a greater length of ceramic insert, necessary to achieve the same overall absorption to achieve the design Q. The DIELEC field profile ("true" cavity) has a more complex structure, and the CASCADE field profile used by MAGYKL is not as good an approximation in this parameter regime. Figure 2 shows the profile of the cavity field for the radial position at which the electron beam travels, for both the true cavity and the equivalent cavity for case B. The effect of the extended dielectric region is apparent, causing a plateau in the field profile. This deviation from the equivalent cavity profile is sufficient to influence the electron beam. Figure 3 shows the transfer function curves calculated by both MAGYKL and MAGYKL-C for this case. It can be seen that MAGYKL and MAGYKL-C differ distinctly in the peak efficiency. Similarly, the efficiency versus frequency dependence as predicted by MAGYKL and MAGYKL-C is different. For this design, it would be necessary to use the new version of the code to be confident of the results. However, in the cases, such as case A, the benefits of the computation speed justify the procedure of using the "cold" field axial profile in MAGYKL without taking into account the effect of the lossy dielectric.

III. DRIFT TUBE DESIGN

Gyroklystron drift spaces ideally provide a field-free environment in which ballistic bunching of the electron beam can occur. As discussed in preceding sections, the drift tube radius is made small enough to ensure that the cavity operating mode is cut off inside the drift tube. However, this does not guarantee that the drift tube is free from the fields asso-
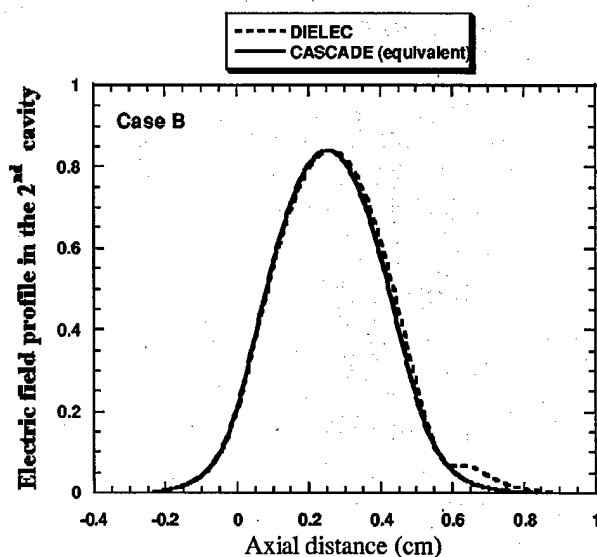

FIG. 2. The cavities' parameters are as follows: Cavity 1 f_c = 92.486 GHz, Q_{ext} = 300, Q_{loss} = 800; the drift length between the first and second cavity $L_{drift,1}$ = 0.64 cm; Cavity 2 length L_2 = 0.5 cm, f_c = 93.494 GHz, Q_{loaded} = 170; the drift length between the second and third cavity $L_{drift,2}$ = 0.82 cm; Cavity 3 length L_3 = 0.5 cm, f_c = 92.917 GHz, Q_{loaded} = 170; the drift length between the third and forth cavity $L_{drift,3}$ = 0.82 cm; Cavity 4 f_c = 93.315 GHz, Q_{loaded} = 338; the dielectric permittivity, $\varepsilon = 10.00 - i0.88$ has a slightly lower real part, permitting greater field penetration, and a smaller loss tangent, so that a larger region of dielectric is necessary to achieve the same value of design Q. This was achieved with the dielectric inserts of width $L_{diel,cav1} = L_{diel,cav2}$ = 0.18 cm. The solid line in the figure is the electric field profile in the second cavity determined by CASCADE. The dashed line in the figure is the electric field profile in the second cavity determined by DIELEC.

ciated with self-oscillation. A simple metal drift tube, bounded by transitions to the gyroklystron cavities on either end, can function as an unintentional resonant cavity to modes different from the normal operating mode. This is particularly true with gyroklystrons operating in the TE_{01} mode, since the lower order TE_{11} mode can propagate at drift
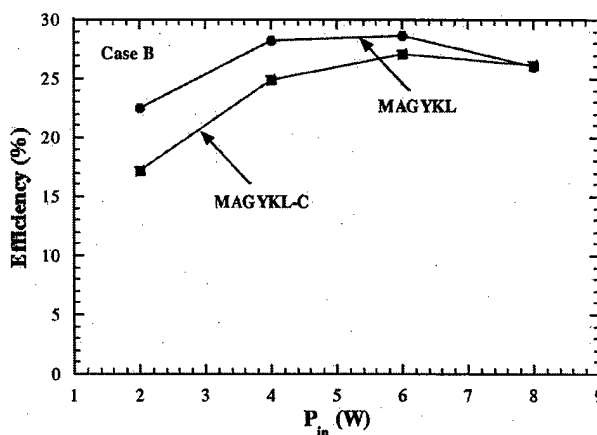

FIG. 3. The transfer curve predicted by MAGYKL (dielectric insert assumed not perturbing the fields in the cavity, hence CASCADE fields are used) and by MAGYKL-C (DIELEC fields are used). The electromagnetic structure parameters are the same as in Fig. 2. The beam parameters are: V = 55 kV, I = 4A, α = 1.5, rms $(\Delta v_\perp / v_\perp)$ = 10%. Magnetic field is 35.8 kG and the drive frequency is 93.45 GHz.

tube radii and frequencies considerably below the limiting values for the TE_{01} mode. These types of instabilities associated with inadvertent drift tube resonators, as well as backward-wave gyro-instabilities in the drift tubes, become increasingly troublesome as one pushes toward higher beam power.

To prevent drift tube oscillations, lossy dielectric materials (absorbers) are placed inside the drift spaces.[15] The absorber consists of a continuous liner of lossy dielectric that covers most of the drift tube length. The extreme ends of the drift tube adjacent to the cavities are metal, to prevent power deposition into the dielectric from leakage fields. Often the dielectric radius is made somewhat larger than the surrounding metal, to help prevent charge buildup from stray electrons from the beam. The procedure for analyzing the stability of a candidate drift tube consists of a number of steps that are applicable to any of the configurations, although the details will depend on the specific structure under investigation. Essentially, one first determines the frequencies where oscillation could occur. This is followed by an evaluation of the attenuation and quality factor of the lossy structure at these frequencies, in comparison to computed start oscillation values. Finally, if needed, the physical dimensions of the drift tube structure can be adjusted to optimize performance in an iterative manner.

To illustrate the procedure, consider placing a liner with a radial thickness of 0.8 mm and a complex dielectric constant of $\varepsilon = 12.24 - i3.67$ around the 1.75 mm drift tube. Provided that the length of the dielectric is at least several wavelengths long, one can ignore edge effects and model the structure as being infinitely long.

Cyclotron maser instabilities are most likely to occur at a frequency where the dispersion curve (a plot of frequency versus axial wave number) of the drift structure intersects with the dispersion curve for Doppler upshifted cyclotron waves supported by the electron beam. When a dielectric liner is placed into the drift tube, two effects occur. First, for modes that can propagate in the empty guide at the frequency of interest, the presence of losses creates a complex propagation factor in the axial direction $\beta = k_z - ik_{zi}$, where the axial variation of fields is assumed to follow the functional form $e^{-j\beta z}$. The term k_{zi} represents an attenuation caused by the losses. The second effect of the dielectric is a significant change in k_z; modes that were originally heavily cut off at the frequency of interest ($k_{zi} > 0$, $k_z = 0$) can often propagate as a result of the addition of dielectric. For the lossy dielectric liner to be effective, it is important that these newly liberated modes receive sufficient attenuation as well. In the same manner, the addition of dielectric also modifies the functional form of the dispersion curve and changes the instability frequencies. The modified dispersion curves for what originally were the TE_{11}, TM_{11}, and TE_{12} modes are shown in Fig. 4, and are now indicated by HE_{11}, HM_{11}, and HE_{12}. This latter notation indicates that the modes are now hybrid (both E_z and H_z components exist). The new HE_{11} backward-wave intersection frequency with the beamline is now at 51.8 GHz, while the forward-wave interaction with this mode is eliminated. However, the HM_{11} and HE_{12} curves have been pulled down to have intersections at 56.0 GHz for
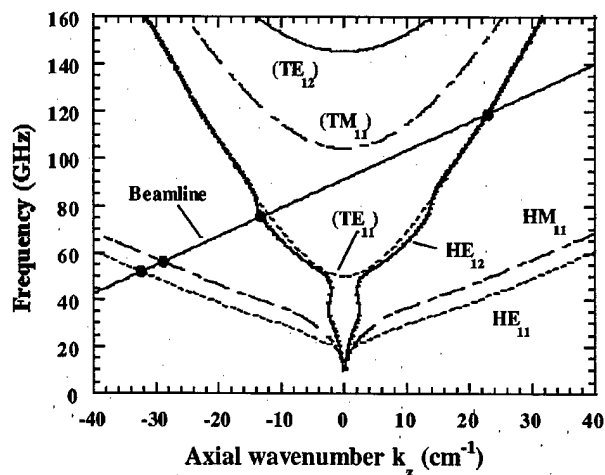

FIG. 4. The dispersion curves are plotted for the TE_{11}, TM_{11}, and TE_{12} modes for $a = 1.75$ mm. The dispersion curve for cyclotron waves on a relativistic beam is given by $\omega = \Omega + k_z v_z$, where Ω is the relativistic cyclotron frequency, k_z is the axial wave number (wave propagation factor), and v_z is the axial beam velocity. It is represented by the straight line in the figure, for the case of a 65 kV beam with a 36.8 kG magnetic field and $\alpha = 1.5$. The modified dispersion curves for what originally were the TE_{11}, TM_{11}, and TE_{12} modes are also shown in the figure, and are now indicated by HE_{11}, HM_{11}, and HE_{12}. This latter notation indicates that the modes are now hybrid (both E_z and H_z components exist).

the backward wave HM_{11}, 75.2 GHz for the backward-wave HE_{12}, and 119.2 GHz for the forward-wave HE_{12}. Having identified the relevant frequencies for beam-wave intersections (and thus potential instabilities), one can now evaluate the stability of the loaded structure.

To better quantify the effect of dielectric on each of the modes, one must realize that is often not the attenuation per unit length that is critical for suppressing oscillation, but rather the quality factor of the inadvertent cavity that can exist within the drift tube. This quality factor will determine whether a particular beam power will trigger oscillation since stability scales as the product of beam power with Q. If the transitions on both ends of the drift tube produced total reflection (a worst-case situation), the dielectric-induced quality factor of such a cavity would be $Q = Q_\Omega = k_z/k_{zi}$. In Fig. 5 the quality factors of the modes are plotted versus frequency. The potential instability frequencies from Fig. 4 are indicated with the circles. One can see that quality factors at the HE_{11}, HM_{11}, and the lower HE_{12} instability frequencies are below 7, which indicates extremely effective loading. Since these values of Q_Ω are massively below the empty beam tunnel starting Q for the design current (about 200), drift tube stability at these intersection frequencies is guaranteed. Because the gyroklystron amplifier will be used in radar, it must be unconditionally stable at the operating point in the cavities as well as the drift tubes. Thus, a linear analysis was used to determine stability conditions in each part of the circuit.[16] More detailed stability analysis is out of the scope of this paper and will be published elsewhere in the future.
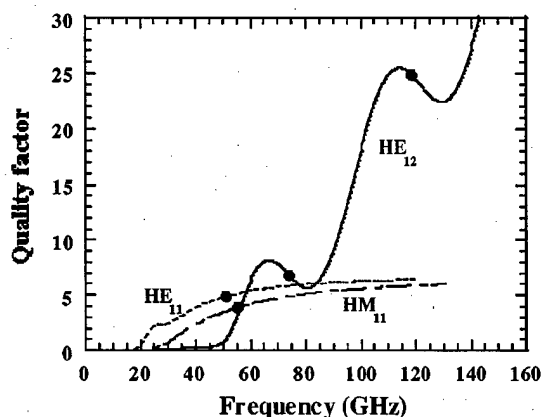
FIG. 5. The quality factors, $Q = k_z/k_{zi}$, of the modes are plotted versus frequency. The potential instability frequencies from Fig. 4 are indicated with the circles.

IV. DESIGN OF THE INPUT COUPLER

The input coupler has to satisfy the following requirements. First, the bandwidth of the coupler should be enough to meet the demands of the gyroklystron bandwidth. Second, the operating mode should be TE_{01} and there should be high degree of mode purity. Third, the amount of power coupled into the TE_{01} mode should be maximized. To meet these requirements we choose a coaxial slotted structure for the input coupler,[17] shown in cross section in Fig. 6. The coupler has the advantage of a single guide feed, good cavity mode purity, minimal ohmic loading of the cavity walls, and it can be designed with a low loaded quality factor.

The input wave guide excites the TE_{411} mode in the outer cavity. Power is coupled through four axial slots to the inner cavity TE_{011} mode. We employed in the design effort two general three-dimensional (3D) codes, HFSS[18] and
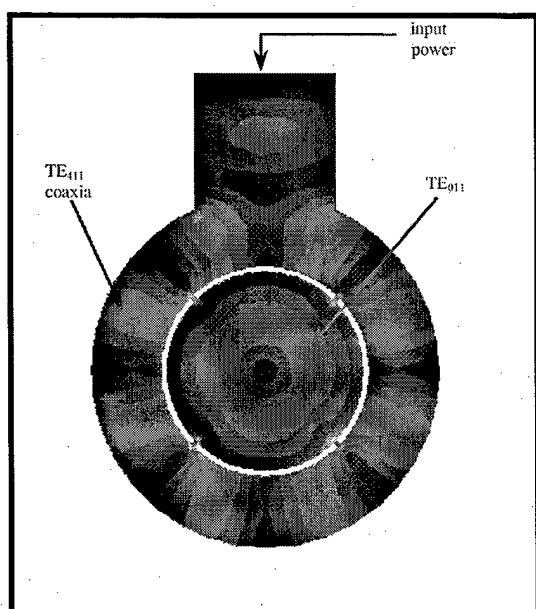

FIG. 6. HFSS simulation of coaxial drive cavity in cross sectional view showing $|E|^2$.

ARGUS.[19] These codes are the only practical tool to investigate the effects of cylinder/coax centerline offsets, coupling slot axial offsets, nonequal slot azimuthal spacing, slot rotations, cavity wall distortions, and other nonideal configurations. These codes are viewed as complementary in their characteristics; each with particular advantages that can be exploited. The tetrahedral modeling elements employed by HFSS conform nicely to structures with curved surfaces, although small "facets" must be used for high accuracy. This results in a large number of unknowns, leading to large problems that strain computational resources. Geometric parameterization is also difficult due to the adaptive meshing, since a geometry change results in a different initial mesh. On the other hand, the ability to transmit a wave through the structure at a particular frequency closely mimics typical testing or operation scenarios. ARGUS clearly identifies the cavity eigenmodes, in contrast to HFSS, where decomposition of the electric field is required to determine mode content. The structured grid of ARGUS results in a "stairstep" approximation of curved surfaces, requiring a dense grid for adequate resolution. ARGUS is somewhat faster, since it can be run on Cray supercomputers, although the overall solution time is comparable to that using HFSS, since multiple runs are required for Q determination. Large problems can be handled with ARGUS, albeit with long solution times. However, parameterization is relatively easy with a structured grid. Finally, the real utility of using both codes for coupler modeling is confidence in the results. The same answers are obtained using two completely different solution approaches. Both codes were used with various methods of solution to model many issues concerning the input coupler, including resonant frequencies, modes, Q's, resistive loading, mode purity, parameterization, and manufacturing tolerances. In particular, ARGUS and HFSS were used to model the Q and resonant frequency for the operating mode of the input coupler. Excellent agreement (0.1%) was achieved between the two codes.

Several techniques were employed with HFSS to determine the resonant frequency and Q of the TE_{01} mode in the cylindrical cavity. The cavity resonant frequency and Q were determined from the frequency dependence of stored energy. The resonant frequency, f_r, is the frequency at maximum stored energy and $Q = f_r/(f_u - f_1)$, where f_u and f_1 are the upper and lower frequencies where the stored energy is half of the maximum value. Specifically, E^*E was calculated over the cavity volume, using the "fast-frequency sweep" option which uses an asymptotic wave form evaluation to calculate a "bandwidth" solution from a full field solution at a single frequency. Excellent agreement with ARGUS results was obtained with a sufficiently high number of polygon segments approximating circular boundaries, ~2°/facet. A second method "de-embeds" S_{11} at the drive port to find the "detuned short" position. The resonant frequency and Q are calculated from the phase of the reflection coefficient. HFSS has also been used to model a "transmission" measurement by launching the TE_{01} mode in the cylindrical cavity by evanescent coupling through the drift tube and "receiving" at the rectangular port.

ARGUS is used in the eigenvalue solver mode. In prin-

ciple, all relevant modes and frequencies can be determined. Since the entire problem volume, including conductors, is meshed, a sector of the configuration is typically modeled for reasonable problem size and solution time. Resonant frequencies and Q's in ARGUS are determined from a variation of the "detuned short" method due to Kroll and Yu[20] requiring multiple runs as the length of the input wave guide is varied. The method of geometry input in ARGUS is more conducive to parametric variation than for HFSS, once the basic geometry has been set. HFSS, on the other hand, can be more quickly set up when major geometry changes are involved. Both HFSS and ARGUS were used to estimate the mode purity of the TE_{011} circular cavity mode. Performance of the input coupler is found using both HFSS and ARGUS to be quite sensitive to dimensions, and the dimensional sensitivity approaches the limits of ordinary manufacturing tolerances. Note that a 0.0003 cm change in cylindrical cavity radius shifts the resonant frequency by ~100 MHz. It is important that the slot angular orientation be within about 1° of the normal value of 45° with respect to the input wave guide. A 1° slot rotation increases f by ~20 MHz and reduces Q by 3%. A 5° slot rotation increases f by ~36 MHz and reduces Q by 30%. A frequency and Q within ±100 MHz and ±50, respectively, of the design values are acceptable from overall circuit performance considerations.

V. SUMMARY

The design of both two and three cavity K_a-band gyroklystron circuits have been validated experimentally.[3,4] The design of the W-band gyroklystron circuits have been validated experimentally with record performance in efficiency, peak power, and bandwidth,[5,6] thereby demonstrating the validity of the design codes and the design methodology. For example, in Fig. 7 (Fig. 8 from Ref. 6) the measured efficiency and peak output power versus frequency are plotted together with the predicted values. The theoretical predictions are in very good agreement with the measured data. In this particular example the W-band gyroklystron circuit performance was designed to mimic the electrical performance of the high average power version of the gyroklystron. Radar applications usually require devices having high peak and average power capabilities. The procedure of the circuit, drift section, and input coupler design described above has been used in designing an industrial version of the NRL W-band gyroklystron, namely a four-cavity gyroklystron capable of operating at 100 kW peak power, with efficiency more than 20% and instantaneous bandwidth of 600 MHz and capable of delivering 10 kW average power.[11] The 3D codes HFSS and ARGUS have been also used to identify the geometry of the intermediate cavities that provides the assumed eigenfrequencies, quality factors, and mode purity, while being consistent with thermal management and material constraints. Furthermore, MAGYKL was used to study variation in circuit performance with changes in circuit dimensions, thus establishing manufacturing tolerances.[21] The thermal management issues for the cavities have been addressed by using the 3D thermomechanical code ANSYS.[22] The performance of the high average power W-band gy-
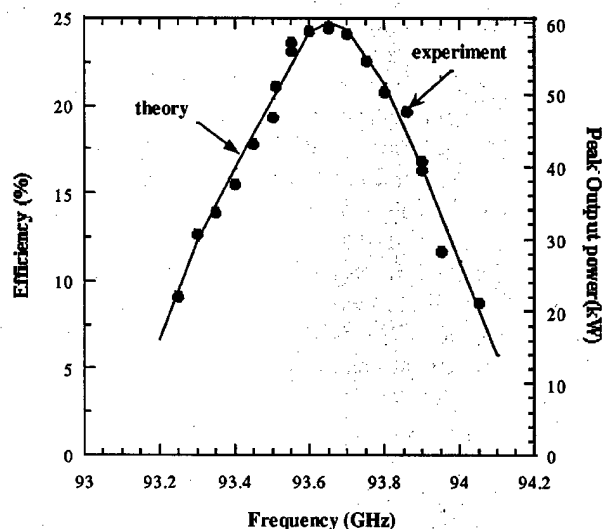

FIG. 7. Theoretical (solid line) and experimental (black circles) peak power and efficiency as a function of drive frequency. Cavity 1 f_c=93.00 GHz, Q_{ext}=150, Q_{loss}=800; Cavity 2 f_c=93.74 GHz, Q_{loaded}=108; Cavity 3 f_c=93.14 GHz, Q_{loaded}=107; Cavity 4 f_c=93.49 GHz, Q_{loaded}=145; Electron beam parameters are: V=57.72 kV, I=4.2A, α=1.5, perpendicular velocity spread, $\Delta v_\perp/v_\perp$=9%. Magnetic field was optimized for maximum efficiency and bandwidth above 600 MHz, B=36.0 kG. The 3 dB bandwidth is 640 MHz.

roklystron will demonstrate the extent of the validity of the entire design methodology, which includes design tools for both electrical and thermomechanical analysis.

[1] I. I. Antakov, A. V. Gaponov, E. V. Zasypkin, E. V. Sokolov, V. K. Yulpatov, L. A. Aksenova, Ap. Keyer, V. S. Musatov, V. E. Myasnikov, L. G. Popov, B. A. Levitan, and A. A. Tolkachev, *Strong Microwaves in Plasmas*, Proceedings of the International Workshop, Moscow–Nizny-Novgorod, 1993 (Nizhny Novgorod University Press, Nizhny Novgorod, 1993), p. 587.
[2] I. I. Antokov, E. V. Zasypkin, and E. V. Sokolov, *Conference Digest, 18th International Conference on Infrared and Millimeter Waves*, Colchester, U.K., 1993, edited by J. R. Birch and T. J. Parker SPIE **2104**, 466 (1994).
[3] J. Calame, M. Garven, J. Choi, K. Nguyen, F. Wood, M. Blank, B. Danly, and B. Levush, Phys. Plasmas **6**, 285 (1999).
[4] J. J. Choi, A. H. McCurdy, F. Wood, R. H. Kyser, J. P. Calame, K. Nguyen, B. G. Danly, T. Antonsen, B. Levush, and R. K. Parker, IEEE Trans. Plasma Sci. **26**, 416 (1998).
[5] M. Blank, B. G. Danly, B. Levush, P. E. Latham, and D. E. Pershing, Phys. Rev. Lett. **79**, 4489 (1997).
[6] M. Blank, B. G. Danly, B. Levush, and D. E. Pershing, IEEE Trans. Plasma Sci. **26**, 409 (1998).
[7] G. Nusinovich, B. Danly, and B. Levush, Phys. Plasmas **4**, 469 (1997).
[8] M. Botton, T. Antonsen, Jr., B. Levush, K. Nguyen, and A. Vlasov, IEEE Trans. Plasma Sci. **26**, 882 (1997).
[9] P. Latham, W. Lawson, and V. Irwin, IEEE Trans. Plasma Sci. **22**, 804 (1994).
[10] W. Lawson, J. P. Calame, B. Hogan, P. E. Latham, M. E. Read, V. L. Granatstein, M. Reiser, and C. D. Striffler, Phys. Rev. Lett. **67**, 520 (1991).
[11] B. G. Danly, M. Blank, J. Calame, B. Levush, K. Nguyen, D. Pershing, J. Petillo, T. Hargreaves, R. True, A. Theiss, G. Good, K. Felch, T. Chu, H. Jory, P. Borchand, B. James, W. Lawson, and T. Antonsen, Jr., "Development of a W-band Gyroklystron for Radars Applications," Conference Digest of the 23rd International Conference on Infrared and Millimeter

Waves, Colchester, September 7–11, 1998, edited by T. J. Parker and S. R. P. Smith (University of Essex, Colchester, 1998), p. 33.

[12] B. Levush and T. Antonsen, Jr., IEEE Trans. Plasma Sci. **18**, 260 (1990).

[13] J. M. Neilson, P. E. Latham, M. Caplan, and W. Lawson, IEEE Trans. Microwave Theory Tech. **37**, 1165 (1989).

[14] A. Gaponov, M. Petelin, and V. Yulpatov, Radiophys. Quantum Electron. **10**, 794 (1967).

[15] J. P. Calame and D. K. Abe, Proc. IEEE **87**, (1999).

[16] P. Latham, S. Miller, and C. Striffler, Phys. Rev. A **45**, 1197 (1992).

[17] G. S. Park, C. Armstrong, R. Kyser, J. Hirshfield, and R. Parker, Int. J. Electron. **78**, 983 (1995).

[18] High Frequency Structures Simulator, Part No. Hewlett-Packard 85180A.

[19] J. Petillo, W. Kreuger, C. Kostas, A. Mondelli, and A. Drobot, "Application of the ARGUS Code in Accelerator Physics," Proceedings of the 1993 Computational Accelerator Physics Conference edited by R. Ryne, AIP Conf. Proc. No. **297** (American Institute of Physics, New York, 1994) p. 303.

[20] N. M. Kroll and D. U. L. Yu, Part. Accel. **34**, 231 (1990).

[21] M. Blank, B. Danly, and B. Levush, IEEE Trans. Plasma Sci. **26**, 409 (1998).

[22] ANSYS Inc., Multi-Purpose Design Analysis Software, Ansoft Corporate Headquarters, Four Station Square, Suite 660, Pittsburgh, PA 15219-1119.